

 Very Important Publication

Switchable Brønsted Acid-Catalyzed Ring Contraction of Cyclooctatetraene Oxide Towards the Enantioselective Synthesis of Cycloheptatrienyl-Substituted Homoallylic Alcohols and Oxaborinanes

Jana Sendra,^a Oriol Salvado,^b Manuel Pedrón,^c Efraim Reyes,^a Tomás Tejero,^d Elena Fernández,^{b,*} Pedro Merino,^{c,*} and Jose L. Vicario^{a,*}

^a Department of Organic and Inorganic Chemistry, University of the Basque Country (UPV/EHU) P.O. Box 644, 48080 Bilbao (Spain)

E-mail: joseluis.vicario@ehu.es

^b Oriol Salvado, Elena Fernández: Department Química Física i Inorgànica, University Rovira i Virgili, C/ Marcel·lí Domingo s/n, 43007 Tarragona (Spain)

E-mail: mariaelena.fernandez@urv.cat

^c Instituto de Biocomputación y Física de Sistemas Complejos (BIFI), Universidad de Zaragoza, 50009 Zaragoza (Spain)

E-mail: pmerino@unizar.es

^d Instituto de Síntesis Química y Catálisis Homogénea (ISQH), Universidad de Zaragoza/CSIC. 50009 Zaragoza (Spain)

Manuscript received: February 6, 2023; Revised manuscript received: February 23, 2023;

Version of record online: March 30, 2023



Supporting information for this article is available on the WWW under <https://doi.org/10.1002/adsc.202300121>

© 2023 The Authors. *Advanced Synthesis & Catalysis* published by Wiley-VCH GmbH. This is an open access article under the terms of the Creative Commons Attribution License, which permits use, distribution and reproduction in any medium, provided the original work is properly cited.

Abstract: The ability of cyclooctatetraene oxide to undergo two sequential ring contraction events under mild conditions, using Brønsted acid catalysis, has been studied in detail. We have found that the selectivity can be controlled by the acidity of the catalyst and by the temperature, being able to obtain selectively either the cycloheptatriene carbaldehyde product, arising from a single ring-contraction event, or phenylacetaldehyde that is formed after a second ring contraction process. A complete mechanistic picture of the reaction and a rationale behind the influence of the catalyst is provided based on both experimental and computational data. Finally, this acid-catalyzed ring contraction has been coupled with an *in situ* enantioselective allylation reaction, delivering enantioenriched cycloheptatrienyl-substituted homoallylic alcohols when it is carried out in the presence of a chiral phosphoric acid catalyst. These homoallylic alcohols have also been converted into enantioenriched oxaborinanes through copper-catalyzed nucleophilic borylation/cyclization protocol.

Keywords: ELF; Organocatalysis; Ring Contraction; Boron; Reaction Mechanisms

Introduction

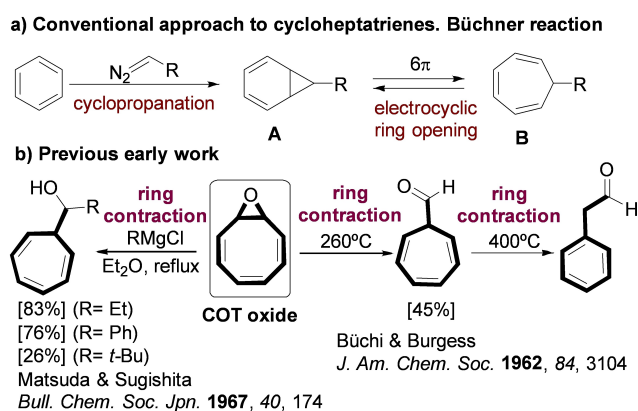
The cycloheptatriene (CHT, homobenzene) scaffold is an intriguing molecular architecture that has attracted the attention of organic chemists due to its particular reactivity profile^[1] and the well-known equilibrium with its valence tautomer norcaradiene (NCD).^[2] In addition, it serves as suitable starting material in the preparation of interesting synthetic targets that incor-

porate seven-membered carbocyclic units within their molecular framework, whose synthesis is a particular challenge by itself due to the more limited number of available reactions that enable the construction of functionalized cycloheptanes.^[3] In this sense, the conventional approach to functionalized cycloheptatrienes makes use of the Buchner reaction that involves metal-catalyzed cyclopropanation of arene derivatives to give the norcaradiene system **A** in equilibrium with

the cycloheptatriene system **B** (Scheme 1).^[4] The **A**:**B** ratio depends on the substituents^[5] and in most occasions **B** has prevalence, although it is not uncommon to find **A** as the major isomer.^[6] Actually, both isomers are connected by a disrotatory 6π electrocyclic ring-opening reaction under thermal conditions, with a highly aromatic transition structure.^[7] More recent investigations based on FMO theory confirms the homoaromaticity of NCD.^[8] As an alternative to the Buchner reaction, very early reports showed that the reaction of cyclooctatetraene oxide (COT oxide) with a handful of Grignard reagents, in refluxing Et_2O , leads to cycloheptatrienes through ring contraction.^[9] However, this reaction is very limited in scope and also phenylacetaldehyde was identified as one of the major side products (see also Scheme 1). Pyrolysis of COT oxide at 260°C provides cycloheptatrienyl carbaldehyde which further evolves to phenylacetaldehyde at temperatures over 400°C ^[10] and another report shows the possibility of tuning the first ring contraction under Rh(I) catalysis at -50°C .^[11]

It has also been shown that acids can promote the transformation of COT oxide into phenylacetaldehyde.^[12] Some of these reports also tried to provide a possible mechanistic rationale for this behavior, making several proposals for the formation of the cycloheptatriene products but mentioning that the formation of phenylacetaldehyde “remains mechanistically obscure and it is conceivable that an acid-catalyzed rather than a thermal process is involved”.^[10] More recent progress in the field has led to other authors to evaluate the reactivity of COT oxide towards other different organometallic reagents, observing that the natural reactivity of this substrate involves conjugate addition rather than direct epoxide ring-opening.^[13]

Considering all these precedents, we decided to explore the reactivity of COT oxide **1**, in the presence of Brønsted acid catalysts with different pKa. The



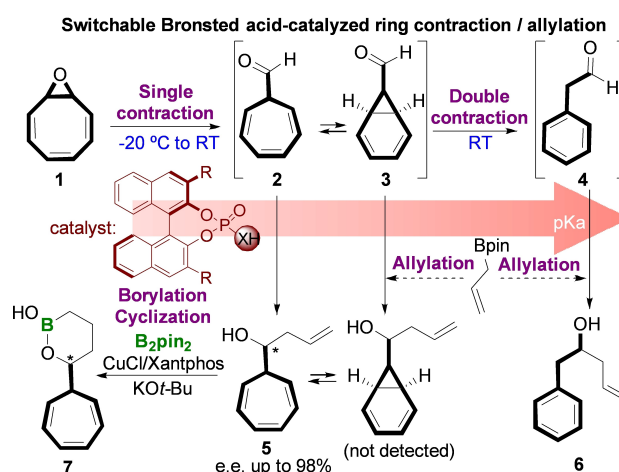
Scheme 1. Conventional approach to cycloheptatrienes and the alternative use of COT oxide described previously.

reaction outcome showed an influence of the pKa along the ring contraction process of **1** generating either cyclohepta-2,4,6-triene-1-carbaldehyde **2** or phenylacetaldehyde **4** (Scheme 2).

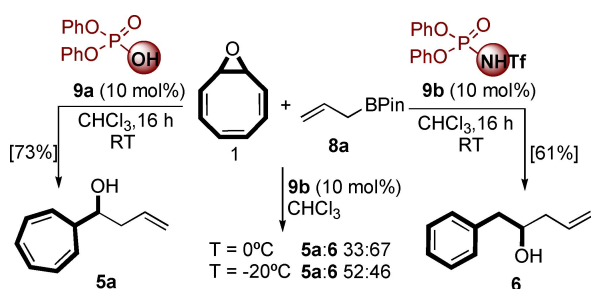
Since Brønsted acids are also known to catalyze the addition of allylboronates to aldehydes,^[14] we also envisaged that this switchable ring contraction could be coupled with an allylation process, incorporating the allylboronate reagent within the reaction medium. In addition, through the participation of a chiral Brønsted acid, the enantioselective access to 1-(cyclohepta-2,4,6-trien-1-yl)but-3-en-1-ol **5** is feasible. Further Cu-catalyzed borylation of the homoallylic alcohol moiety allows its transformation into enantioenriched oxaborinanes **7** incorporating the valuable cyclohepta-trienyl substituent in the heterocycle, with stereo-retention (Scheme 2).

Results and Discussion

We started our work by evaluating the performance of different Brønsted acid catalysts in the ring contraction/allylation of COT oxide **1**, using allylborane **8a**, in toluene as solvent at room temperature, as the model system (Scheme 3). Our first experiments directly showed that the reaction in the presence of diphenylphosphoric acid (catalyst **9a**) generated exclusively the cycloheptatriene-containing allylic alcohol **5a**. On the other hand, when we employed the more acidic diphenylphosphoramidate catalyst (**9b**), the reaction furnished alcohol **6** without detecting any trace of compound **5a** in the crude reaction mixture. It should also be noticed that the reaction catalyzed by **9b** leading to product **6** was found to be faster than the one under **9a** catalysts, that provided **5a**.



Scheme 2. Switchable acid catalyzed COT oxide ring contraction/allylation towards enantioselective homoallylic alcohols and oxaborinanes.



Scheme 3. Reaction optimization with a model system. Reactions at 0 °C and –20 °C were conducted until total consumption of the starting material.

Interestingly, when the reaction was carried out at lower temperature using **9b** as catalyst, mixtures of **5a** and **6** were obtained. This result might suggest some sort of kinetic/thermodynamic control; however when either pure **5a** or mixtures of **5a/6** were stirred in the presence of 10 mol% of **9b**, at ambient temperature for 16 h, the reactants remained unaltered, concluding that the reaction was not reversible and the thermodynamic control can be discarded to justify the observed regioselectivity. In fact, the **5a/6** ratio observed at 0 °C and –20 °C pointed out that aldehyde **2** might be an intermediate in the formation of **4**, both undergoing irreversible allylation. In this context, the reaction was investigated by NMR and using DFT methods. On the other hand, the mixture of **1** and **8a**, without any Brønsted acid catalyst, did not evolve towards any product, recovering all starting materials unchanged (see ESI for details), which rules out the possible participation of the boronate reagent as Lewis acid promoter of the ring contraction processes.

Mechanistic studies. Preliminary ¹H-NMR experiments were carried out monitoring the reaction in absence of the allyl reagent to locate the intermediate aldehydes. First, COT oxide **1** was treated with 10 mol% of each catalyst in CDCl₃ and ¹H-NMR spectra were recorded at varying reaction times (Figure 1).

These experiments show that when catalyst **9a** was employed, the formation of cycloheptatriene carboxaldehyde intermediate **2** could be observed, increasing its concentration as the reaction evolved. Actually, as reported before,^[6a] compound **2** is accompanied by a considerable proportion of its valence tautomer **3** and an average spectrum is observed. The same experiment using catalyst **9b** showed the instantaneous disappearance of substrate **1** and the clean formation of phenylacetaldehyde **4** after 10 min. Remarkably, aldehyde **2** can be observed in the initially registered ¹H NMR spectrum, which showed the presence of both aldehydes **2** and **4** in an almost 1:2 ratio after 2 min, pointing towards the possibility that aldehyde **2** might

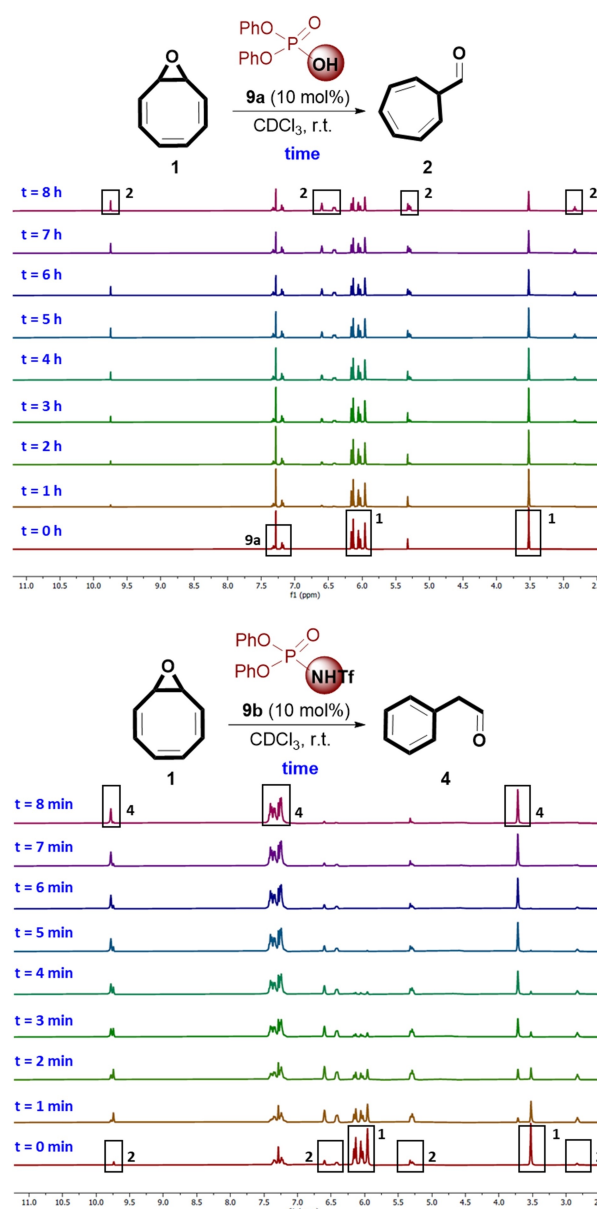
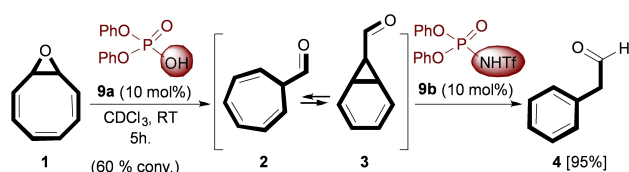


Figure 1. ¹H-NMR spectra of the crude reaction mixture of COT oxide **1** with 10 mol% of catalyst **9a** (top) and **9b** (bottom).

be converted into **4** by the action of the stronger Brønsted acid catalyst.

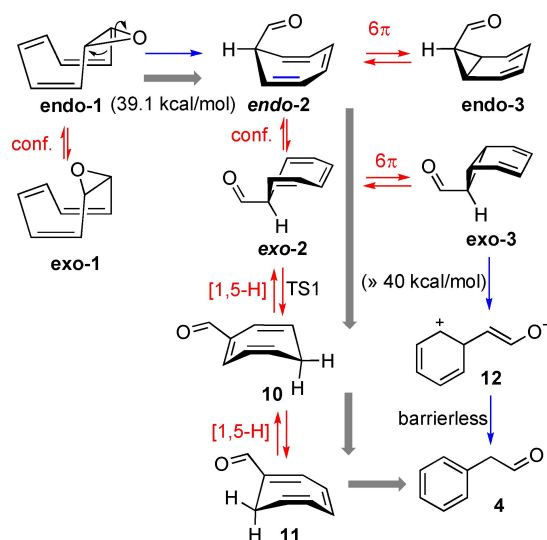
For this reason, and in a different experiment (Scheme 4), COT oxide **1** was subjected to the **9a**-catalyzed ring contraction reaction under the standard conditions, also in the absence of allylboronate **8a**. After 5 h, ¹H NMR analysis of the crude reaction mixture showed a 60% conversion of the starting material into aldehyde **2** without observing any formation of aldehyde **4**. Next, the catalyst **9b** (10 mol%) was added at once to this mixture, leading to the clean formation of phenylacetaldehyde **4** and without detecting any trace of aldehyde **2**. This experi-



Scheme 4. Catalyst switch experiment for successive single and double ring contraction.

ment demonstrates that aldehyde **2** (or its valence isomer **3**) undergoes conversion into **4** in the presence of a strong Brønsted acid such as **9b**, supporting the reaction sequence illustrated in Scheme 2.

We next carried out a computational study of this transformation at DFT level (all discussed energies are free energies; for details see SI). We first studied the neutral approach reported by Buchi and Burguess^[10] who suggested the formation of **4** through the grey (full arrows) route depicted in Scheme 5, i.e. contraction of **1** to **2** which lead to species **10**, then to **11** and finally to **4**. The compound *exo*-**3** was captured through a Diels-Alder reaction.^[10] Compounds **2**, **10**, and **11** are subjected to the CHT-NCD isomerism mentioned above. We located the transition structure for the first step and verified the connection between **1** and *endo*-**2** through the corresponding IRC, which showed the presence of a hidden intermediate (see below). The barrier for this transformation was found to be of 39.1 kcal/mol. On the other hand, the energy barrier for the formation of the valence tautomer *endo*-**3** was found to be of only 9 kcal/mol. In any case, the barrier of 39.1 kcal/mol precludes completely the possibility of the neutral route under our reaction



Scheme 5. Proposed pathway for the conversion of **1** into **4**. Grey route proposed in ref. [10]. Blue processes are favoured and red processes are disfavoured in acidic media.

conditions. Therefore, we then moved to study the acid-catalyzed reaction. (For a detailed study of the neutral mechanism see SI).

When the transformation of **1** into *endo*-**2** was calculated in the presence of **9a** (See Figure 2), the barrier (**TS1a**) was found to be 22.6 kcal/mol. For the isomerization between *endo*-**2** and *endo*-**3** through a 6 electrocyclic reaction the barrier (**TS2a**) was found to be 8.7 kcal/mol. The IRC of **TS1a** identified *endo*-**1** as the starting point and *endo*-**2** as the final point but it showed the presence of a plateau, longer than that found in the neutral model (Figure 2a and SI), which is characteristic of the presence of a hidden intermediate,^[15] according to our experience.^[16]

Thus, we decided to study in detail the evolution of the electron density along the reaction coordinate to determine accurately how **1** was transformed into **2**. For that purpose, we carried out the analysis of the electron localization function (ELF)^[17] along the entire IRC of the reaction (Figure 2a–c). The ELF analysis allows to analyze the concertedness of a reaction by establishing the moment in which a given bond is broken or formed. The evolution of electron density illustrated in Figure 2a describes the situation summarized in Figure 2b and allows to assign the predominating species in each moment. The transient carbocations **A** and **B** can be detected and characterized from the relevant points of the ELF analysis showing the descriptors (maxima of electron population) that allow identifying the moment in which a bond is formed or broken (Figure 2c) (For details of the ELF analysis see SI).

In addition, when complemented with an analysis of non-covalent interactions (NCI),^[18] it can also be employed to evaluate changes in the electronic population of bonds and atoms with lone pairs as well as to analyze transient species. According to the ELF analysis, the full concerted process can be divided into six series of events defined by changes in the electron population represented along the IRC (Figure 2a). Directed molecular dynamics provides information related to reaction time, thus allowing assign a lifetime to the different species. Thus, we also performed quasi-classical direct dynamic calculations,^[19] using the software PROGDYN,^[20] to estimate the half-time in which hidden intermediates exist (Figure 2d). We assigned half-life times of 60 and 30 fs for **A** and **B**, respectively (for details see SI). The ELF analysis also demonstrates that a complete proton transfer should take place prior to the oxirane ring-opening; in other words, protonation is necessary for the first step of the reaction, confirming that the pKa of the acid catalyst is a key factor. In our case, the acidity is implicit in the model since we calculate the whole system (substrate + acid) and not the protonated or deprotonated form without considering the counterion. In the presence of catalyst **9b**, the energy barrier found for the first step

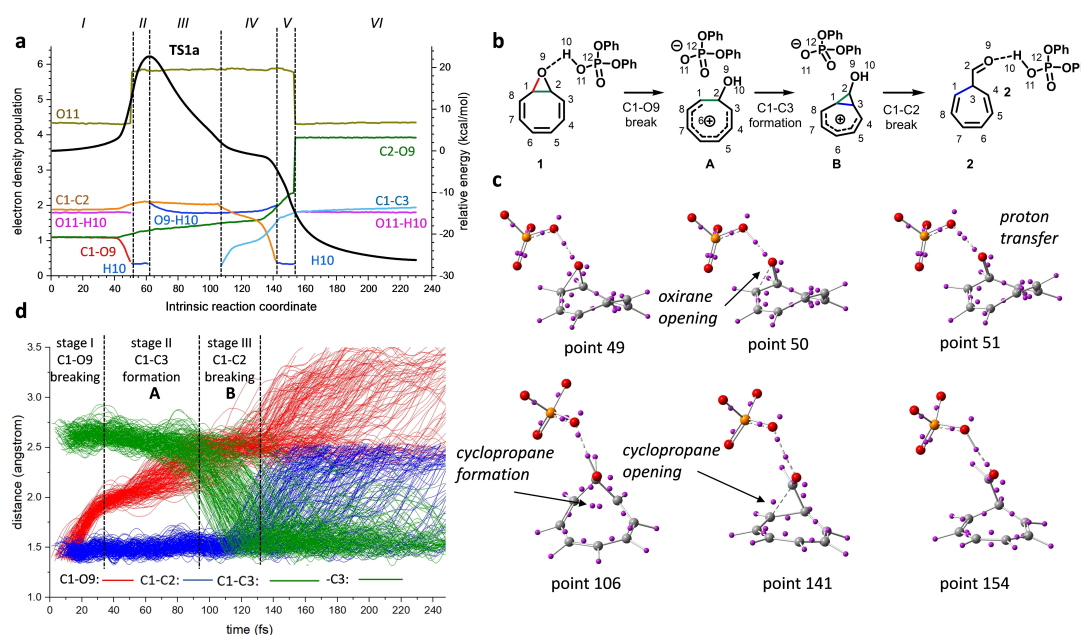
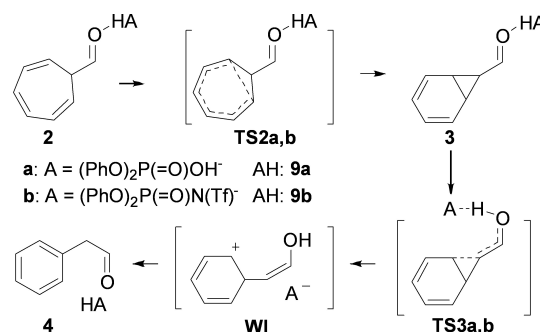


Figure 2. Analysis of the reaction coordinate corresponding to the transformation of **1** into **2**. (a) ELF analysis. Black trace represents the intrinsic reaction coordinate IRC. Colored lines indicate the electron population of the basin corresponding to the indicated bond or atom (lone pairs). (b) Representation of hidden carbocationic intermediates (transient species) **A** and **B** during the transformation of **1** into **2** corresponding to cleavage and formation of key bonds. (c) Representative points with descriptors (purple balls indicating maxima of electron population) of the IRC showing oxirane opening (points 49 and 50), formation of the cyclopropane (point 106) and opening of the cyclopropane (point 141) to give compound **2** (point 154). Phenyl rings have been omitted for clarity. (d) Quasi-classical direct dynamic simulations. Representations of C1–O9 (red), C1–C2 (blue), and C1–C3 (green) bonds for 180 trajectories from **TS1a**. When only C1–C2 is formed the transient carbocation **A** is present, formation of C1–C3 indicates the presence of transient carbocation **B**, and finally, breaking of C1–C2 provides intermediate **2**.

(**TS1b**) was 21.9 kcal/mol, similar to **TS1a**. We also conducted an ELF analysis for this reaction as well as dynamic simulations and similar results to those of the reaction catalyzed by **9b** were obtained (for details see SI). The only difference between both ELF analyses is that in the case of **9b** the proton transfer takes place instantaneously which is consistent with the lower pKa of **9b** with respect to **9a**.^[21]

The optimized geometries of **TS1a** and **TS1b** are shown in Figure 3. It can be observed a larger distance from nitrogen to the proton (1.58 Å) in **9b** than from the phosphate oxygen to the proton (1.42 Å) in **9a**, confirming the higher acidic character of the former and that, at the transition state structure, the proton-transfer is more advanced for the more acidic catalyst **9b**. This is confirmed by a NCI analysis that showed a partial proton transfer in the case of **9a** and a complete proton transfer in the case of **9b** (Figure 3, bottom).

The second part of the reaction consists on the evolution of aldehyde **2** towards phenylacetaldehyde **4** (Scheme 6). This transformation should take place through the valence tautomer **3** and it was suggested for the neutral mechanism under harsh reaction conditions ($T > 250^\circ\text{C}$) that cannot preclude the formation of radicals. However, in the presence of acid



Scheme 6. Mechanistic proposal for the transformation of **2** into **4**.

catalysts **9a** or **9b** the transformation takes place smoothly.

The isomerization of **2** into **3** takes place through **TS2a,b** with barriers of 7.9 and 8.4 kcal/mol for the reactions in the presence of **9a** and **9b**, respectively. We have considered isomerization from the major *exo* isomer of compound **2**. (For details on the *endo/exo* conformational equilibrium in **2** see SI). Actually, the acids do not catalyze the reaction, as it is indicated by the preference of the deprotonated form in the transition structure (see below). On the other hand, the

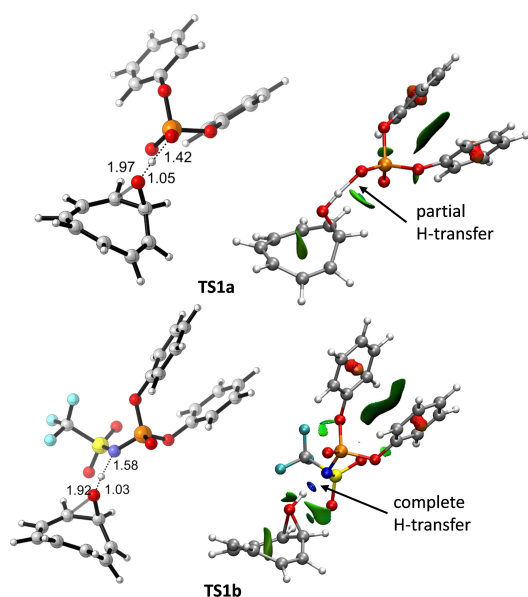


Figure 3. Left: Optimized (wb97xd/def2svp, SMD=chloroform) geometries of transition structures **TS1a** and **TS1b**, corresponding to the formation of aldehyde **2** from **1** catalysed by **9a** and **9b**, respectively. Right: NCI analysis showing non-covalent interactions. Thin, green surface indicates van der Waals interactions. Small, lenticular, bluish surfaces indicate strong interactions such as hydrogen bonding.

next step, the cyclopropane ring-opening, requires protonation of the aldehyde to activate the system (ring-opening in the neutral form requires more than 40 kcal/mol, see SI). The ring-opening catalyzed by **9a** showed a barrier of 23.6 kcal/mol and that catalyzed by **9b** of 16.3 kcal/mol, 7.3 kcal/mol lower, therefore reflecting a process favored by the most acidic catalyst. Noteworthy, the formation of **4** is only possible from compound **3**, and there is no route from isomer **2**. The resulting Wheeland intermediate **WI** formed through **TS3a,b** evolves to the enol in a barrierless process and then aldehyde **4** is obtained. The optimized geometries for the corresponding transition structures are given in Figure 4 and clearly reflect that isomerization of cycloheptatriene carbaldehyde **2** to formyl norcaradiene **3** takes place through the deprotonated form since the proton is located at the catalyst. On the contrary, transition structures **TS3a,b** correspond to the protonated form of the substrate, as required for promoting the cyclopropane ring-opening.

The analysis of the energy profiles of the process (Figure 5) revealed that, while the rate limiting stage of the process for the reaction catalyzed by **9a** is the formation of aldehyde **4** from **3** (23.6 kcal/mol), through **TS3a**, in the case of the reaction catalyzed by **9b**, the rate-limiting stage is the first step (**TS1b**), with a barrier of 21.9 kcal/mol. The difference between the two reactions is of 1.7 kcal/mol in favor of that catalyzed by the most acidic catalyst **9b**.

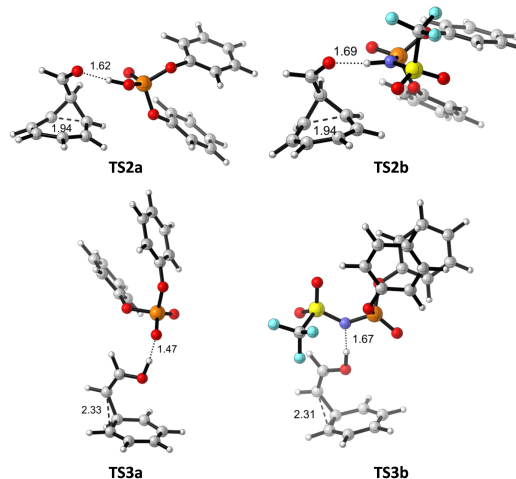


Figure 4. Optimized (wb97xd/def2svp/SMD=chloroform) geometries of the transition structures **TS2a,b** and **TS3a,b**. Note that while in **TS2a,b** the proton is located in the catalyst, in **TS3a,b** the proton is located in the substrate.

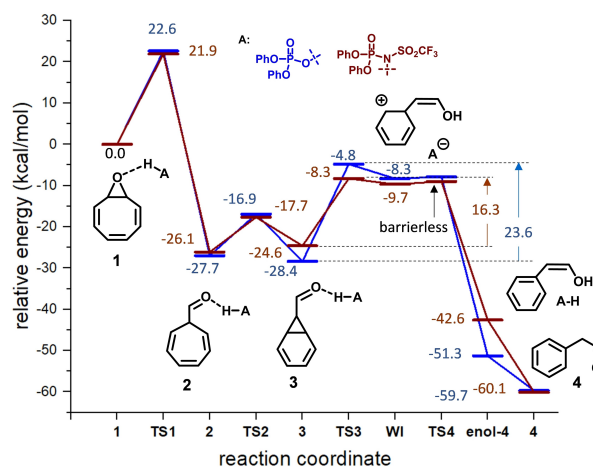


Figure 5. Energy profile for the transformation of **1** into **2** and then **4**, catalyzed by **9a,b**.

This difference is enough to justify the different behavior observed for the two catalysts but also the formation of mixtures when temperature is lowered. The different rate-limiting stage for the two reactions is also in agreement with the experimental observations in the absence of allylating reagent, for which, at RT, aldehyde **2** only is accumulated when the reaction is catalyzed by **9a**. This profile also justifies the experimental results observed when the reaction is carried out in the presence of allyl boronate **8a** although the allylation reaction also needs to be studied (see below).

In order to support the above mechanism with different rate-limiting steps depending on the acidity of the catalyst, and to provide quantitative experimental values for the rate constants, we carried out kinetic

studies of the conversion of compound **1** into aldehydes **2** and **4** (Figure 6). For that purpose we performed two reactions using 10 mol% of each catalyst (**9a** and **9b**) at ambient temperature. The reactions were monitored by ^1H NMR (For details see SI). Figure 6 illustrates the kinetics for the transformation of **1** catalyzed by **9a** (top) and **9b** (bottom).

The reaction was carried out in the absence of allylboronate, to evaluate the evolution of compound **2**. The process showed the typical situation corresponding to two consecutive reactions (**1** leading to **2** and then to **4**) with comparable rate constants.^[22] The equilibrium between **2** and **3** should also be considered; according to calculations the valence tautomers are close in energy with a barrier of 7–8 kcal/mol, enough low to consider them in equilibrium. In fact, as mentioned above, in NMR spectra we see the average signals between **2** and **3**, as reported.^[6] At ambient temperature, there is a considerable difference in the rate of the reaction when catalyzed by **9a** (slow) and by **9b** (fast). The obtained experimental values for the rate constants were in excellent agreement with the barriers showed in Figure 6. For the reaction catalyzed by **9a**, the first step is faster ($k_1 = 1.82 \cdot 10^{-5} \text{ s}^{-1}$) than the second one ($k_2 = 6.31 \cdot 10^{-6} \text{ s}^{-1}$), which corresponds to a barrier of 24.5 kcal/mol according to Eyring's equation (calculated 23.6 kcal/mol). On the contrary,

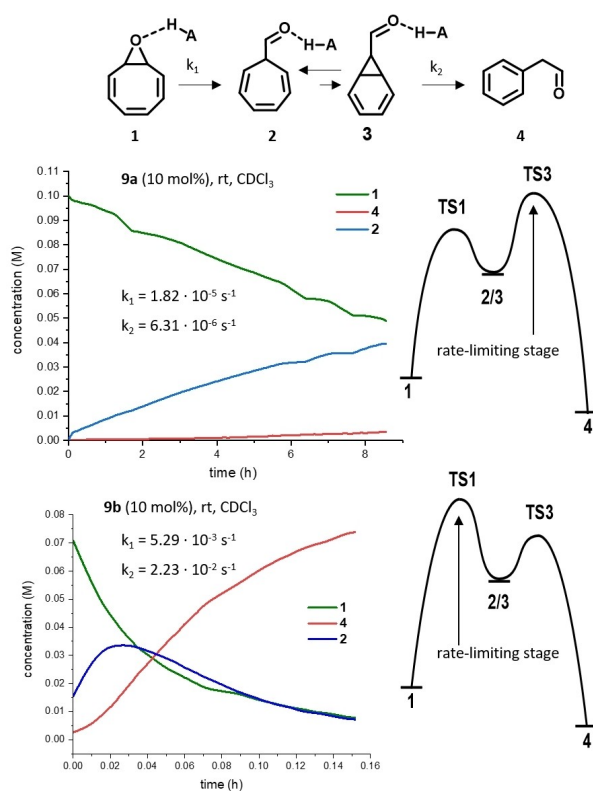
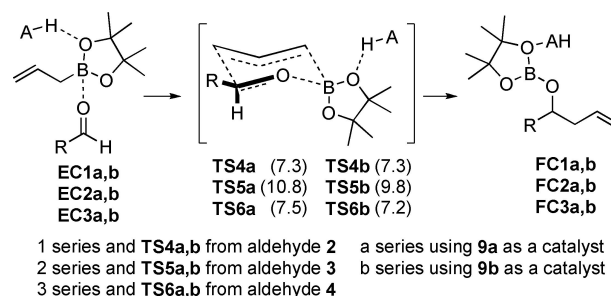


Figure 6. Isomerization of **1** in the presence of **9a** (top) and **9b** (bottom).

for the reaction catalyzed by **9b** the first step is slower ($k_1 = 5.29 \cdot 10^{-3} \text{ s}^{-1}$) corresponding, with a barrier of 20.6 kcal/mol according to Eyring's equation (calculated 21.9 kcal/mol) than the second one ($k_2 = 2.23 \cdot 10^{-2} \text{ s}^{-1}$). In both cases, the difference between calculated and experimental values is within the admitted error for DFT (1–2 kcal/mol).^[23] Additionally, we monitored reactions at 50 °C for the reaction catalyzed by **9a** and at 0 °C for the reaction catalyzed by **9b** to verify that aldehyde **2** is always an intermediate. In fact, the reaction catalyzed by **9a** at 50 °C becomes faster and it could be observed the formation of aldehyde **4** at the expense of aldehyde **2**. The reaction catalyzed by **9b**, registered at 0 °C, became slower and it was possible to observe the formation of aldehyde **2**, which is immediately consumed to form **4** (See SI).

We next turned to study the energetic profile of the allylboration of aldehydes **2**, **3** and **4**. This reaction has already been studied computationally with an excellent detail including enantioselective additions by Goodman and co-workers,^[24] who established the general model for the interactions between reactants and the Brønsted acid catalyst during the addition process. According to that model, the allyl boronate coordinates the carbonyl oxygen to reach a classical cyclic six-membered transition state in which the phosphoric acid establishes a H-bond interaction with a boronate oxygen (Scheme 7). (for details see SI). In consequence, this reaction requires for a deprotonated aldehyde and therefore the availability of the deprotonated form in the presence of the different catalysts should also be considered in addition to the corresponding barriers associated to the allylboration step.

We located the transition structures corresponding to the allylation of aldehydes **2**, **3** and **4** in the presence of **9a** (**TS4a–T6a**, respectively) and **9b** (**TS4b–TS6b**, respectively). The obtained barriers for the allylation were found to be 7.3 kcal/mol for the allylation of **2** in the presence of either **9a** or **9b**; 10.8 and 9.8 kcal/mol for the allylation of **3** in the presence



Scheme 7. Calculation of the allylation reactions from the corresponding encounter complexes **EC** to the final complexes **FC**. (Barriers correspond to free energies and are given in kcal/mol relative to the corresponding encounter complex).

of **9a** and **9b**, respectively; and 7.5 and 7.2 kcal/mol for the allylation of **4** in the presence of **9a** and **9b**, respectively. These values clearly indicate a very low dependence of the acidity of the catalyst for the allylation reaction. Representative **TS4a**, **TS5a** and **TS6b**, corresponding to the observed allylations, are illustrated in Figure 7 (for more details see SI). The calculated barrier values are in good agreement with the experimental observations. The lower barrier observed for the allylation process with respect to the rate-determining step associated to the conversion of **1** into **2** indicates that such a reaction is the preferred one, provided that a minimum concentration of deprotonated aldehyde is available. In the case of the reaction catalyzed by **9a** the lower acidity^[21] of the catalyst provides enough deprotonated form and the allylation reaction can proceed without problems (pKa of phosphoric acids like **9a** are in the range of 12–14). On the other hand, in the case of the reaction catalyzed by **9b** (pKa's assigned for mixed imides of phosphoric and triflic acids like **9b** are in the range of 6–7),^[21] the aldehyde is essentially 100% protonated and, consequently, the allylation step is significantly lowered down, allowing for aldehyde **2** to isomerize to **3** and then to aldehyde **4**, which in the presence of allylboronate and without competitive reactions, is finally allylated. Therefore, this is the favored situation in each case: In the reaction catalyzed by **9a**, aldehyde **2** is accumulated facilitating the allylation reaction. In the reaction catalyzed by **9b** in which the first step (formation of aldehyde **2**) is the rate-limiting stage and aldehyde **2** cannot be accumulated, it isomerizes to **4** as it is formed in the protonated form, precluding any background reaction of the deprotonated form (10 mol% of catalyst is used).

Given the crucial role of the acidity of the catalyst in the reaction, we also decided to evaluate the outcome of the reaction using catalysts of different acidity with the aim to establish a correlation between the selectivity of the reaction and the pKa of the Brønsted acid catalyst. As it is shown in Figure 8 a

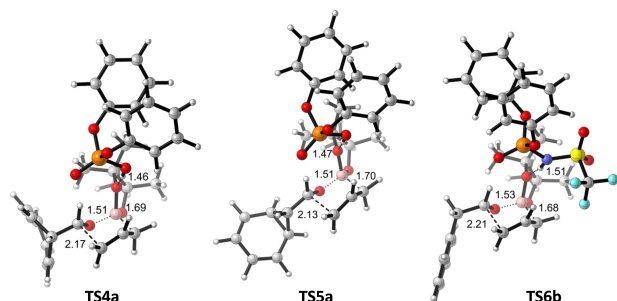


Figure 7. Optimized (wb97xd/def2svp/SMD = chloroform) geometries of the transition structures corresponding to the allylboronation.

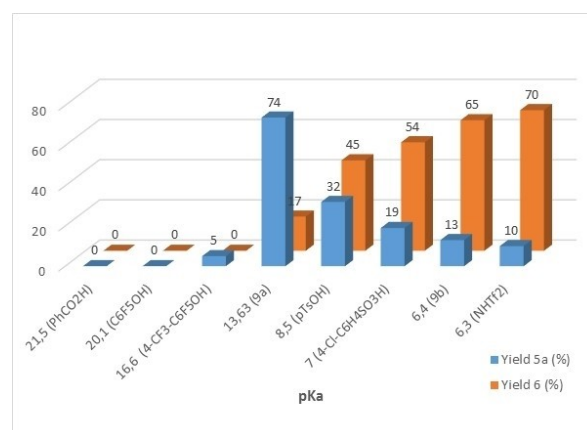


Figure 8. Correlation of catalyst acidity vs selectivity in the acid-catalyzed ring contraction of **1**.

clear trend was observed in the reactions, observing that a catalyst of a certain acidity is needed to start the reaction, since benzoic acid (pKa = 21.5) and perfluorophenol (pKa = 20.1)^[25] were unable to transform **1** into any of the ring contraction products **5a** or **6**, and only observing little conversion of **1** into **5a** when 4-CF₃C₆H₄OH was employed (pKa = 16.6) after prolonged reaction time. With catalyst **9a** (pKa = 13.63) complete disappearance of **1** was observed in 12 h and as a result of the increased catalyst acidity, the formation of phenylacetaldehyde **4** as the product of the double ring contraction process gained prevalence on the reaction mixture.

Stereoselective one pot construction of cycloheptatrienyl-substituted homoallylic alcohols. With the mechanistic studies in hand and in view that, as already mentioned, BINOL-derived chiral Brønsted acids are also known to catalyze the enantioselective addition of allylboronates to aldehydes,^[14] we became interested on developing an enantioselective version of this ring contraction/allylation sequence. This would enable a direct and easy synthesis of cycloheptatrienyl-substituted homoallylic alcohols **5** from a readily available starting material such as COT oxide **1**. We have not considered the possibility of developing the double ring contraction followed by enantioselective allylation to produce enantioenriched 1-phenylpent-4-en-2-ols, such as **6**, since their preparation can be conducted using commercially available phenylacetaldehyde **4** through the same type of chiral Brønsted acid-catalysed allylation.^[26]

Considering the reactivity between **1** and **8a** as the model reaction system, we first proceeded to evaluate a variety of BINOL-based chiral phosphoric acids in order to identify the optimized one in terms of asymmetric induction. For the initial experiments, we decided to carry out the reaction in a solvent of low polarity such as toluene, in order to maximize the

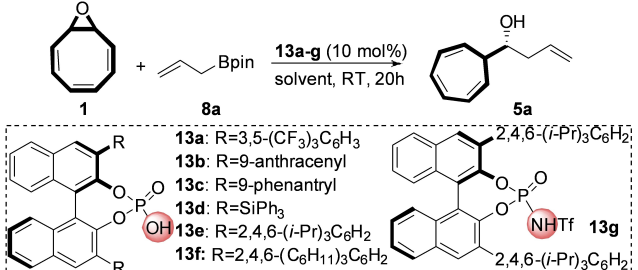
potential H-bonding interactions between the catalyst and the substrates that would contribute to higher enantioselectivities. As it can be seen in Table 1, from the different chiral BINOL-based phosphoric acids tested (entries 1–6), the archetypical TRIP-phosphoric acid **13e** provided the highest enantioselectivity (entry 5). We also evaluated phosphoramidate **13g** (entry 7), which also provided adduct **5a** with comparable high enantioselectivity, although the reaction was contaminated with minor amounts of phenylacetaldehyde addition product **6**. Unfortunately, this was isolated as a racemic material. We next evaluated the influence of the solvent on the reaction (entries 8–16) observing

that other arenes such as mesitylene or xylene provided slightly lower enantioselectivities (entries 8 and 9) while chloroform, used in our previous mechanistic experiments, provided a more promising 82% ee (entry 10). When more polar solvents such as Et₂O or AcOEt were used (entries 11 and 12) the reaction was much less efficient, not only with respect to enantiocontrol but also in terms of chemical yield.

In view of the better performance of the reaction in chloroform, several other halogenated solvents were tested (entries 13–16), being able to slightly increase the enantioselectivity of the process using 1,2-dichloroethane and also observing the quantitative formation of **5a** (entry 14). Working at slightly lower temperature enabled increasing the ee to 86% (entry 17) but when the reaction was carried out at 0 °C, it became extremely slow, not observing significant conversion after 24 h of reaction (entry 18). Finally, the ee of adduct **5a** could be further increased to 89% ee by working at higher concentration (entry 19) and maintaining the excellent yield of the reaction. The absolute configuration of **5a** was assigned based on mechanistic analogy with the already reported data for the enantioselective allylation of aldehydes catalyzed by phosphoric acids described in the literature^[14a] and the stereochemical model provided by Goodman.^[24]

With an optimized protocol in hand, we proceeded next to evaluate the scope of this ring contraction/enantioselective allylation sequence by using allylboronates with different substitution patterns (Table 2). As it can be seen in this table, (*E*)-crotylboronate **8b** performed excellently in the reaction, providing the corresponding homoallylic alcohol **5b** quantitatively and as an almost exclusive *anti*-diastereoisomer with very high enantiomeric excess (entry 2). Remarkably, the stereoisomer (*Z*)-crotylboronate **8c** also underwent clean addition leading to the formation of the *syn*-configured adduct **5c** as a single diastereoisomer and an excellent ee (entry 3). When γ -substituted allylboronates with bulkier substituents were employed, the reaction also proceeded with high yields and complete diastereoselectivity in all cases, although the enantioselectivity of the process became significantly affected as the size of this substituent increased (entries 4 and 5) and a similar situation was found when cinnamylboronate **8f** was tested in the reaction (entry 6). Cyclic α,γ -disubstituted boronate **8g** provided a moderate yield of the addition product presumably due to the inherent instability of this boronate reagent, but adduct **5g** was again isolated as a single diastereoisomer of very high enantiomeric purity (entry 7). We also tested the challenging γ,γ -disubstituted allylboronate **8h** in this reaction, and we proved the quantitatively synthesis of compound **5h** with high enantiocontrol (entry 8). On the other hand, β -substituted boronate reagent **8i** furnished product **5i** with low ee, even though the ring contraction/addition process was

Table 1. Optimization of the enantioselective acid-catalyzed ring contraction/allylation^[a]



Entry	Catalyst	Solvent	T [°C]	Yield [%] ^[b]	ee [%] ^[c]
1	13a	Toluene	RT	89	24
2	13b	Toluene	RT	79	54
3	13c	Toluene	RT	78	34
4	13d	Toluene	RT	46	12
5	13e	Toluene	RT	67	82
6	13f	Toluene	RT	62	64
7	13g	Toluene	−20	70 ^[d]	76
8	13e	Mesitylene	RT	65	64
9	13e	<i>o</i> -xylene	RT	68	72
10	13e	CHCl ₃	RT	86	82
11	13e	Et ₂ O	RT	15	10
12	13e	AcOEt	RT	< 5	n.d. ^[e]
13	13e	CH ₂ Cl ₂	RT	99	82
14	13e	Cl(CH ₂) ₂ Cl	RT	99	84
15	13e	PhCF ₃	RT	99	80
16	13e	PhCl	RT	99	82
17	13e	Cl(CH ₂) ₂ Cl	15	99	86
18	13e	Cl(CH ₂) ₂ Cl	0	< 5	n.d. ^[e]
19 ^[f]	13e	Cl(CH ₂) ₂ Cl	15	99	89

^[a] Reaction carried out in a 0.1 mmol scale of **1**, with 10 mol% of **13a–f** and 1.1 eq. of **8a** in the indicated solvent (1 mL) and temperature, until complete consumption of **1** (TLC analysis).

^[b] Yields of pure isolated products after flash column chromatography.

^[c] ee was determined by HPLC analysis.

^[d] Compound **6** was also obtained in 28% yield and as a racemic material.

^[e] n.d. = not determined.

^[f] Reaction carried out at 1.5 M concentration of **1**.

Table 2. Scope of the Brønsted acid catalyzed ring contraction/enantioselective allylation.^[a]

Entry	allylborane	Product	Yield [%] ^[b]	dr ^[c]	ee [%] ^[d]
1			99	–	89
2			99	>20:1	93
3			90	>20:1	98
4			92	>20:1	78
5			89	>20:1	66
6			99	>20:1	55
7			58	>20:1	88
8			86	–	86
9			99	–	28
10			95	–	80

^[a] Reaction carried out in a 0.2 mmol scale of **1**, with 10 mol% of **13e** and 1.1 eq. of boronate **8a–j** in 1,2-dichloroethane (0.13 mL) at 15 °C for 16 h.

^[b] Yields of pure isolated products after flash column chromatography.

^[c] Determined by ¹H-NMR analysis of crude reaction mixture.

^[d] ee was determined by HPLC analysis.

highly efficient in terms of chemical yield (entry 9). Finally, we also evaluated allenylboronate **8j** as a potential nucleophile in the reaction, leading to homopropargyl alcohol **5j** in high yield and remarkable enantioselectivity (entry 10).

Computational calculations using the Goodman model were also carried out with the real chiral catalysts **13e** and **13g** (Figure 9). We selected as a model reaction the addition of allyl boronate **8a** to aldehydes **2** (TS7a,b), **3** (TS8a,b), and **4** (TS9a,b) in the presence of **13e** and **13g** (both *Re* and *Si* faces were explored as well as the conformational variability of the transition structures, making a total of 36 transition structures) and full convergence, the most stable 12 transition structures were obtained. From all these approaches, we could only verify experimentally the allylation of aldehyde **2** when the reaction is carried out in the presence of **13e** and the allylation of aldehyde **4** when the reaction is carried out in the presence of **13g**. In the case of the reaction with **13e** calculations predicted the enantiomer coming from a

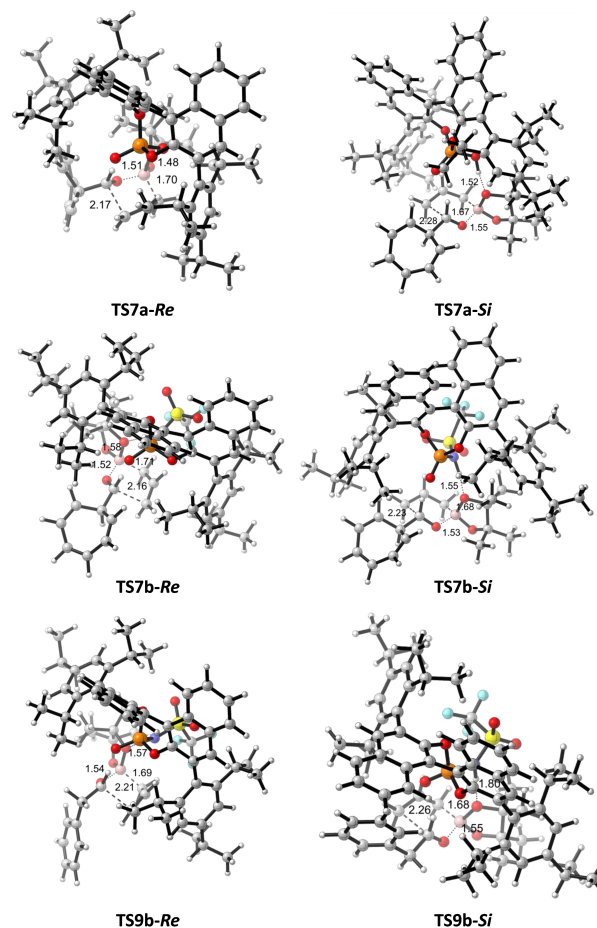
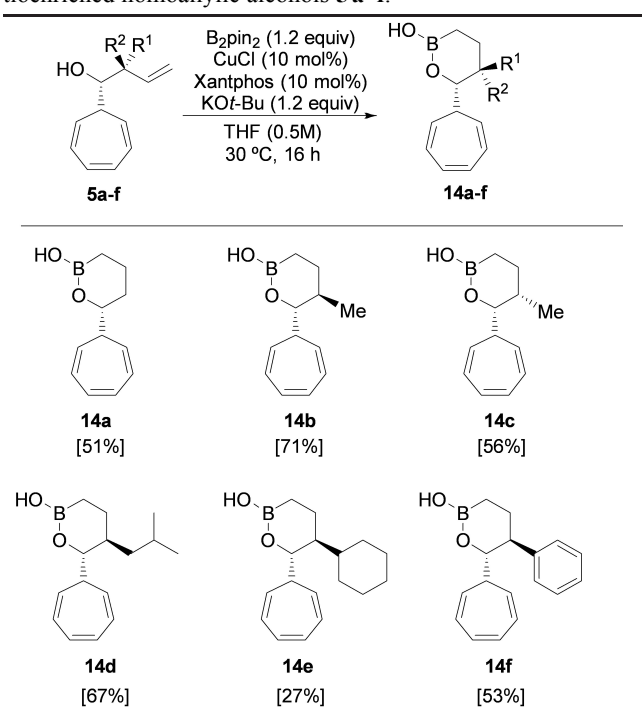


Figure 9. Optimized (wb97xd/def2svp/SMD=chloroform) geometries of the transition structures corresponding to the allylation.

Re attack to be predominant with the possibility of obtaining a minor amount of the other enantiomer (difference between the transition structures **TS7a-Re** and **TS7a-Si** of 3.0 kcal/mol, Figure 9). This result is in an excellent agreement with 89% ee found experimentally. In the case of the allylation in the presence of **13g**, calculations predict a good enantioselectivity for the allylation of aldehyde **2** (difference of 2.5 kcal/mol for **TS7b-Re** and **TS7b-Si** in favor of the *Re* attack) and a practically racemic mixture for the allylation of aldehyde **4** (difference of 0.5 kcal/mol between **TS9b-Re** and **TS9b-Si**), as it is experimentally seen.

Stereoselective synthesis of oxaborinanes. Once we had optimized the synthetic approach to enantioenriched homoallylic alcohols **5**, containing the cycloheptatrienyl moiety, we conducted next their transformation into oxaborinanes through copper catalyzed nucleophilic pinacolboranyl (Bpin) addition to the terminal double bond,^[27] with concomitant intramolecular OH attack to the Bpin moiety. We first explored this reaction using the enantioenriched homoallylic alcohol **5a** as model substrate, and proceeded to evaluate the reaction conditions for borylcupration of terminal alkenes already reported by us (Table 3).^[28] Under

Table 3. Stereoselective synthesis of oxaborinanes from enantioenriched homoallylic alcohols **5a-f**.^[a]



^[a] Reaction carried out in a 0.15 mmol scale of homoallylic alcohol **5a-f**, with 10 mol% of $CuCl$, 10 mol% of Xantphos, 1.2 equiv. of B_2pin_2 and 1.2 equiv. of $KOt-Bu$ in THF (0.5 M) at 30 °C, 16 h. Yields refer to isolated products after flash column chromatography purification.

these conditions, we were able to isolate oxaborinane **14a** in 51% isolated yield in an overall process that, remarkably, involved a fully chemoselective borylcupration, towards the terminal C=C double bond, not affecting the triene unit of the cycloheptatrienyl moiety.

We next extended this study to a family of representative examples of homoallylic alcohols **5**, starting with methyl-substituted homoallylic alcohols **5b** and **5c**, that were generated from the allylboranes **8b** (*E* isomer) and **8c** (*Z* isomer) respectively. In these two cases, we were able to synthesize the corresponding oxaborinanes **14b** and **14c** in good yields under these optimized conditions, and the assignment of the *trans*- or *cis*-configuration for both of them was established by ¹D-NMR NOE experiments. This stereoretentive behavior for this reaction is in agreement with the stereochemical outcome proposed by Murakami and coworkers on their previous report dealing with the enantioselective synthesis of *anti*-1,2-oxaborinan-3-enes from aldehydes and 1,1-di(boryl)alk-3-enes in the presence of ruthenium and chiral phosphoric acid catalysts.^[29] The synthesis of the oxaborinanes from homoallylic alcohols containing isopropyl and cyclohexyl substituents (adducts **5d** and **5e** respectively) was also feasible obtaining compounds **14d** and **14e** and therefore demonstrating the compatibility of these reaction conditions with more hindered substituents on the α -position with respect to the cycloheptatrienyl moiety. Finally, 1-(cyclohepta-2,4,6-trien-1-yl)-2-phenylbut-3-en-1-ol **5f** could also be converted into oxaborinane **14f** in 53% isolated yield.

Conclusion

The ability of cyclooctatetraene oxide **1** to undergo single or double ring contraction processes under Brønsted acid catalysis can be modulated through the pK_a of the chosen catalyst leading selectively to cycloheptatriene carbaldehyde **2** or phenylacetaldehyde **6** in a switchable manner. In addition, when this ring contraction is *in situ* coupled with an allylation reaction process represents a straightforward method for the synthesis of enantioenriched cycloheptatrienyl-substituted homoallylic alcohols, particularly when a BINOL-based chiral phosphoric acid is used as catalyst. These homoallylic alcohols could be conveniently transformed into enantioenriched cycloheptatrienyl-substituted oxaborinanes, via stereoretentive Cu-catalyzed borylcupration/cyclization protocol. A series of control experiments together with computational studies have determined that the mechanism of isomerization of oxirane **1** into aldehyde **2** takes place through a concerted processes in which hidden intermediates are formed. The high dependence of the reaction with the pK_a of the catalysts is also well-

understood by introducing the whole system in the calculations, which also serve to determine that isomerization requires full-protonated species and it takes place from the norcaradiene isomer. Calculations also predict correctly the different effect exerted by the acid catalysts, assigning different rate determining stages to each catalyst of different pKa. These predictions have been corroborated by kinetic studies, which showed rate constants in good agreement with the predicted values. Finally, computational evaluation of the transition structures, corresponding to the enantioselective allylation reaction, also provided results that are in an excellent agreement with those observed experimentally.

Experimental Procedures

Enantioselective ring contraction/allylation reaction. Synthesis of (R)-1-(cyclohepta-2,4,6-trien-1-yl)but-3-en-1-ol (5a): To an oven-dried screw-top vial, equipped with a magnetic stirring bar, catalyst **13e** (15 mg, 0.02 mmol) was added under Ar atmosphere. Then, epoxide **1** (24 mg, 0.20 mmol) was added as a solution in ClCH₂CH₂Cl (0.13 mL), followed by the dropwise addition of boronic ester **8a** (41 μL, 0.22 mmol). The reaction was left stirring at 15 °C for 16 h. The solvent was evaporated under reduced pressure and purification by flash column chromatography (petroleum ether/EtOAc 8:2) afforded **5a** (32.4 mg, 0.20 mmol) in 99% yield as a colourless oil. ¹H-NMR (δ, ppm) (300 MHz, CDCl₃): 6.72–6.58 (m, 2H), 6.26 (dddd, *J* = 21.4, 9.5, 4.4, 1.3 Hz, 2H), 5.85 (dddd, *J* = 16.8, 10.2, 8.0, 6.3 Hz, 1H), 5.48 (dd, *J* = 9.5, 5.8 Hz, 1H), 5.28 (dd, *J* = 9.5, 5.9 Hz, 1H), 5.22–5.09 (m, 2H), 3.92 (ddd, *J* = 8.5, 7.2, 3.5 Hz, 1H), 2.56–2.39 (m, 1H), 2.32–2.17 (m, 1H), 1.81–1.73 (m, 2H). ¹³C-NMR (δ, ppm) (75.5 MHz, CDCl₃): 134.4, 131.0, 130.7, 125.6, 125.4, 122.5, 122.4, 118.5, 70.8, 44.9, 39.7. [α]_D²⁰: –44.8 (*c* = 1.0, CH₂Cl₂). IR (ATR) cm^{–1}: 3390, 3012, 1275, 1260, 994, 916, 749, 701. MS (EI, 70 eV) *m/z* (%): 129 (2), 128 (2), 121 (2), 120 (1), 119 (1), 115 (2), 104 (1), 103 (10), 102 (1), 93 (2), 92 (25), 91 (100), 90 (1), 89 (3), 79 (2), 78 (3), 77 (10), 66 (2), 65 (12), 64 (1), 63 (4), 62 (1), 55 (1), 53 (1), 52 (1), 51 (3), 50 (1). HRMS (ESI) *m/z*: [M–H₂O+H]⁺ Calcd for C₁₁H₁₃ 145.1012; Found 145.1015. The enantiomeric excess was determined by HPLC using a CHIRALPAK® AD-3 column (hexane/*i*-PrOH 90:10, 1 mL/min, 251 nm, 25 °C); *t*_r (major) = 5.67 min, *t*_r (minor) = 6.00 min (89% ee).

Borylation/cyclization. Synthesis of (R)-6-(cyclohepta-2,4,6-trien-1-yl)-1,2-oxaborinan-2-ol (14a): In a glovebox, an oven dried Schlenk tube with a magnetic stirring bar, was charged with CuCl (2.0 mg, 0.02 mmol), B₂pin₂ (60.9 mg, 0.24 mmol), Xantphos (11.6 mg, 0.02 mmol) and KOtBu (26.9 mg, 0.24 mmol). The tube was sealed with the Teflon cap and was connected to a vacuum/Ar manifold out of the glovebox. Next, alcohol **5a** (32 mg, 0.20 mmol), dissolved in THF (0.5 mL, 0.4 M), was added to the main solution, under Ar atmosphere. The reaction was stirred at 30 °C for 16 h. After that, the reaction mixture was filtered through a small pad of Celite® and the solvent was evaporated under reduced pressure. Purification by column chromatography afforded **14a** (19.00 mg, 0.1 mmol) by flash column chromatography (pentane/Et₂O 10:1) in 51%

yield as a yellowish oil. ¹H-NMR (δ, ppm) (400 MHz, CDCl₃): 6.72–6.61 (m, 2H), 6.31–6.16 (m, 2H), 5.44 (dd, *J* = 9.5, 5.5 Hz, 1H), 5.31–5.23 (m, 1H), 4.26 (ddd, *J* = 9.4, 6.6, 2.7 Hz, 1H), 4.02 (br s, 1H), 1.90–1.77 (m, 2H), 1.71–1.61 (m, 1H), 1.56–1.40 (m, 2H), 1.10–0.96 (m, 1H), 0.90–0.74 (m, 1H). ¹³C-NMR (δ, ppm) (100 MHz, CDCl₃): 131.2, 130.7, 125.3, 125.2, 123.1, 122.5, 76.6, 45.6, 31.1, 19.4. ¹¹B-NMR (δ, ppm) (128.3 MHz, CDCl₃): 32.2 (br s). [α]_D²⁰: –12.7 (*c* = 1.0, CH₂Cl₂). MS (EI, 70 eV) *m/z* (%): 190 (M⁺, 11), 189 (4), 175 (4), 147 (8), 146 (3), 131 (13), 129 (6), 128 (5), 125 (4), 121 (3), 120 (3), 119 (4), 118 (13), 117 (46), 116 (7), 115 (24), 105 (12), 104 (23), 103 (13), 102 (4), 99 (46), 98 (14), 93 (3), 92 (13), 91 (100), 90 (3), 89 (6), 79 (8), 78 (11), 77 (21), 71 (7), 67 (3), 66 (3), 65 (18), 63 (8), 56 (4), 55 (93), 54 (3), 53 (6), 52 (4), 51 (10), 50 (3). HRMS (ESI) *m/z*: [M–H][–] Calcd for C₁₁H₁₄BO₂ 189.1092; Found 189.1088.

Acknowledgements

Grants PID2019-104090RB-I00, PID2019-109674GB-I00 and PID2020-118422GB-I00 funded by MCIN/AEI/10.13039/501100011033 and by “ESF Investing in your future” are gratefully acknowledged together with the Basque Government (Grupos IT1558-22) and the Government of Aragón (Grupos Consolidados, E34_20R and a fellowship to M. P.). O. S. thanks MF-URV for a predoctoral grant and J. S. thanks Grant PRE2018-083532 funded by MCIN/AEI/10.13039/501100011033 and by “ESF Investing in your future” for an FPI fellowship. The authors thankfully acknowledge the resources from the supercomputers “Memento” and “Cierzo” and technical expertise and assistance provided by BIFI-ZCAM (Universidad de Zaragoza, Spain).

References

- [1] For some illustrative reviews: a) O. A. McNamara, A. R. Maguire, *Tetrahedron* **2011**, *67*, 9–40; b) H. Jansen, J. C. Slootweg, K. Lammertsma, *Beilstein J. Org. Chem.* **2011**, *7*, 1713–1721; c) M. L. H. Green, D. K. P. Ng, *Chem. Rev.* **1995**, *95*, 439–453.
- [2] a) W. G. Woods, *J. Org. Chem.* **1960**, *23*, 110–112; b) A. A. Jarzeczki, J. Gajewski, E. R. Davidson, *J. Am. Chem. Soc.* **1999**, *121*, 6928–6935; c) A. R. Maguire, P. O’Leary, F. Harrington, S. E. Lawrence, A. J. Blake, *J. Org. Chem.* **2001**, *66*, 7166–7177.
- [3] For some selected general reviews: a) S. A. Blaszczyk, D. A. Glazier, W. Tang, *Acc. Chem. Res.* **2020**, *53*, 231–243; b) T. V. Nguyen, J. M. Hartmann, D. Enders, *Synthesis* **2013**, *45*, 845–873; c) M. A. Battiste, P. M. Pelphrey, D. L. Wright, *Chem. Eur. J.* **2006**, *12*, 3438–3447; d) H. Butenschön, *Angew. Chem. Int. Ed.* **2008**, *47*, 5287–5290; *Angew. Chem.* **2008**, *120*, 5367–5370; e) K. E. O. Ylijoki, J. M. Stryker, *Chem. Rev.* **2013**, *113*, 2244–2266; f) H. Pellissier, *Adv. Synth. Catal.* **2011**, *353*, 189–218; g) M. Harmata, *Chem. Commun.* **2010**, *46*, 8886–8903; h) A. G. Lohse, R. P. Hsung, *Chem. Eur. J.* **2011**, *17*, 3812–3822; i) Z. Yin, Y. He, P. Chiu, *Chem. Soc. Rev.* **2018**, *47*, 8881–8924.

- [4] Pioneering reports: a) E. Buchner, T. Curtius, *Ber. Dtsch. Chem. Ges.* **1885**, *18*, 2377–2379; b) E. Buchner, *Ber. Dtsch. Chem. Ges.* **1896**, *29*, 106–109; For a review: c) S. E. Reisman, R. R. Nani, S. Levin, *Synlett* **2011**, 2437–2442.
- [5] L. M. Bateman, O. A. McNamara, N. R. Buckley, P. O’Leary, F. Harrington, N. Kelly, S. O’Keeffe, A. Stack, S. O’Neill, D. G. McCarthy, A. R. Maguire, *Org. Biomol. Chem.* **2015**, *13*, 11026–11038.
- [6] a) M. Balci, H. Fischer, H. Günther, *Angew. Chem. Int. Ed.* **1980**, *19*, 301–302; *Angew. Chem.* **1980**, *92*, 316–317; b) G. Boche, R. Eiben, *Tetrahedron Lett.* **1985**, *26*, 1289–1292.
- [7] Z. Chen, H. Jiao, J. I. Wu, R. Herges, S. B. Zhang, P. von R. Schleyer, *J. Phys. Chem. A* **2008**, *112*, 10586–10594.
- [8] P. Saini, P. Bhasin, R. K. Bansal, *Comput. Theor. Chem.* **2013**, *1017*, 72–77.
- [9] a) T. Matsuda, M. Sugishita, *Bull. Chem. Soc. Jpn.* **1967**, *40*, 174–177; b) M. Ogawa, M. Sugishita, M. Takagi, T. Matsuda, *Tetrahedron* **1975**, *31*, 299–304. There is also another example showing the possibility of using LiMe₂Cu in this reaction, but other different cuprates provided mixtures of products. (See ref. 13a).
- [10] a) G. Büchi, E. M. Burgess, *J. Am. Chem. Soc.* **1962**, *84*, 3104–3109; The reaction of cyclooctatetraene under oxidative conditions has also been described to provide ring-contraction products b) A. C. Cope, B. Tiffany, *J. Am. Chem. Soc.* **1951**, *73*, 4158–4161; c) A. C. Cope, N. A. Nelson, D. S. Smith, *J. Am. Chem. Soc.* **1954**, *76*, 1100–1104.
- [11] R. Gigg, R. Hayes, A. Sweeney, *J. Chem. Soc. Chem. Commun.* **1971**, 1248–1249.
- [12] C. R. Ganellin, R. Petit, *J. Chem. Soc.* **1958**, 576–581.
- [13] a) F. Del Moro, P. Crotti, V. Di Bussolo, F. Macchia, M. Pineschi, *Org. Lett.* **2003**, *5*, 1971–1974; b) M. Pineschi, F. Del Moro, P. Crotti, F. Macchia, *Eur. J. Org. Chem.* **2004**, 4614–4620; c) O. Yahiaoui, A. Almass, T. Fallon, *Chem. Sci.* **2020**, *11*, 9421–9425; d) M. J. Miller, M. H. Lyttle, A. Streitwieser, *J. Org. Chem.* **1981**, *46*, 1977–1984.
- [14] Pioneering example: a) P. Jain, J. C. Antilla, *J. Am. Chem. Soc.* **2010**, *132*, 11884–11866. For some other selected examples see b) C. H. Xing, Y. X. Liao, Y. Zhang, D. Sabarova, M. Bassous, Q. S. Hu, *Eur. J. Org. Chem.* **2012**, *2012*, 1115–1118; c) L. Clot-Almenara, C. Rodríguez-Esrich, L. Osorio-Planes, M. A. Pericas, *ACS Catal.* **2016**, *6*, 7647–7651; d) S. Fustero, E. Rodríguez, R. Lázaro, L. Herrera, S. Catalán, P. Barrio, *Adv. Synth. Catal.* **2013**, *355*, 1058–1064; e) S. Gao, M. Duan, Q. Shao, K. N. Houk, M. Chen, *J. Am. Chem. Soc.* **2020**, *142*, 18355–18368; f) S. Gao, M. Duan, J. Liu, P. Yu, K. N. Houk, M. Chen, *Angew. Chem. Int. Ed.* **2021**, *60*, 24096–24106; *Angew. Chem.* **2021**, *133*, 24298–24308; g) P. Barrio, E. Rodríguez, K. Saito, S. Fustero, T. Akiyama, *Chem. Commun.* **2015**, *51*, 5246–5249; h) J. Liu, M. Chen, *Org. Lett.* **2020**, *22*, 8967–8972; i) Y. L. Zhang, B. J. He, Y. W. Xie, Y. H. Wang, Y. L. Wang, Y. C. Shen, Y. Y. Huang, *Adv. Synth. Catal.* **2019**, *361*, 3074–3079; j) B. E. Hetzler, G. Volpin, E. Vignoni, A. G. Petrovic, G. Proni, C. T. Hu, D. A. Trauner, *Angew. Chem. Int. Ed.* **2018**, *57*, 14276–14280; *Angew. Chem.* **2018**, *130*, 14472–14476; k) J. Park, Y. Jung, J. Kim, E. Lee, S. Y. Lee, S. H. Cho, *Adv. Synth. Catal.* **2021**, *363*, 2371–2376; l) C. A. Incerti-Pradillos, M. A. Kabeshov, A. V. Malkov, *Angew. Chem. Int. Ed.* **2013**, *52*, 5338–5341; *Angew. Chem.* **2013**, *125*, 5446–5449. See also ref. 26.
- [15] E. Kraka, D. Cremer, *Acc. Chem. Res.* **2010**, *43*, 591–601.
- [16] a) E. Capel, M. Rodríguez-Rodríguez, U. Uria, M. Pedron, T. Tejero, J. L. Vicario, P. Merino, *J. Org. Chem.* **2022**, *87*, 693–707; b) A. Ortega, R. Manzano, U. Uria, L. Carrillo, E. Reyes, T. Tejero, P. Merino, J. L. Vicario, *Angew. Chem. Int. Ed.* **2018**, *57*, 8225–8229; *Angew. Chem.* **2018**, *130*, 8357–8361.
- [17] a) A. Savin, R. Nesper, S. Wengert, T. F. Fässler, *Angew. Chem. Int. Ed.* **1997**, *36*, 1808–1832; *Angew. Chem.* **1997**, *109*, 1892–1918; b) A. Savin, *J. Chem. Sci.* **2005**, *117*, 473–475; c) B. Silvi, I. Fourre, M. E. Alikhani, *Monats. Chem.* **2005**, *136*, 855–879.
- [18] a) E. R. Johnson, S. Keinan, P. Mori-Sanchez, J. Contreras-Garcia, A. J. Cohen, W. Yang, *J. Am. Chem. Soc.* **2010**, *132*, 6498–6506; b) N. Gillet, R. Chaudret, J. Contreras-Garcia, W. Yang, B. Silvi, J.-P. Piquemal, *J. Chem. Theory Comput.* **2012**, *8*, 3993–3997; c) R. A. Boto, F. Peccati, R. Laplaza, C. Quan, A. Carbone, J.-P. Piquemal, Y. Maday, J. Contreras-García, *J. Chem. Theory Comput.* **2020**, *16*, 4150–4158.
- [19] Z. Yang, K. N. Houk, *Chem. Eur. J.* **2018**, *24*, 3916–3924.
- [20] B. R. Ussing, C. Hang, D. A. Singleton, *J. Am. Chem. Soc.* **2006**, *128*, 7594–7607.
- [21] The pK_a’s of BINOL-derived chiral phosphoric acids have been assigned according to literature data. Whereas the pK_a’s of phosphoric acids like **9a** are in the range of 12–14, the pK_a’s assigned for mixed imides of phosphoric and triflic acids like **9b** are in the range of 6–7. See: K. Kaupmees, N. Tolstoluzhsky, S. Raja, M. Rueping, I. Leito, *Angew. Chem. Int. Ed.* **2013**, *52*, 11569–11572; *Angew. Chem.* **2013**, *125*, 11783–11786.
- [22] D. Ball, *J. Chem. Educ.* **1998**, *75*, 917–918.
- [23] A. N. Bootsma, S. E. Wheeler, *ChemRxiv* **2019**. DOI: 10.26434/chemrxiv.8864204.v5.
- [24] M. N. Grayson, S. C. Pelegrinet, J. M. Goodman, *J. Am. Chem. Soc.* **2012**, *134*, 2716–2722.
- [25] A. Kütt, S. Tshepelevitsh, J. Saame, M. Lõkov, I. Kaljurand, S. Selberg, I. Leito, *Eur. J. Org. Chem.* **2021**, *2021*, 1407–1419.
- [26] See ref. 14a. See also a) J. Yuan, P. Jain, J. C. Antilla, *J. Org. Chem.* **2020**, *85*, 12988–13003; b) J. Yuan, P. Jain, J. C. Antilla, *J. Org. Chem.* **2022**, *87*, 8256–8266.
- [27] a) J. Cid, H. Gulyas, J. J. Carbo, E. Fernández, *Chem. Soc. Rev.* **2012**, *41*, 3558–3570; b) H. Gulyas, A. Bonet, C. Pubill-Ulldemolins, C. Sole, J. Cid, E. Fernández, *Pure Appl. Chem.* **2012**, *84*, 2219–2231.

- [28] a) K. Kubota, E. Yamamoto, H. Ito, *J. Am. Chem. Soc.* **2013**, *135*, 2635–2640; b) E. Yamamoto, R. Kojima, K. Kubota, H. Ito, *Synlett* **2015**, *26*, 272–276; c) A. Whyte, B. Mirabi, A. Torelli, L. Prieto, J. Bajohr, M. Lautens, *ACS Catal.* **2019**, *9*, 9253–9258; d) J. Royes, S. Ni, A. Farre, E. La Cascia, J. J. Carbó, A. B. Cuenca, F. Maseras, E. Fernández, *ACS Catal.* **2018**, *8*, 2833–2838; e) R. J. Maza, J. Royes, J. J. Carbó, E. Fernández, *Chem. Commun.* **2020**, *56*, 5973–5976.
- [29] T. Miura, J. Nakahashi, W. Zhou, Y. Shiratori, S. G. Stewart, M. Murakami, *J. Am. Chem. Soc.* **2017**, *139*, 10903–10908.
-